First-principles study of the nano-scaling effect on the electrochemical behavior in $LiNi_{0.5}Mn_{1.5}O_4$

2013 Nanotechnology 24 424007

(http://iopscience.iop.org/0957-4484/24/42/424007)

IOP Publishing Nanotechnology
Nanotechnology **25** (2014) 159501 (1p) doi:10.1088/0957-4484/25/15/159501

Corrigendum: First-principles study of the nano-scaling effect on the electrochemical behavior in $LiNi_{0.5}Mn_{1.5}O_4$ (2013 *Nanotechnology* 24 424007)

Eunseok Lee and Kristin A Persson

Environmental Energy Technologies Division, Lawrence Berkeley National Laboratory, CA 94720, USA

E-mail: eunseoklee@lbl.gov

Received 4 March 2014
Accepted for publication 4 March 2014
Published 20 March 2014

We have found that the surface energy values in table 1 omitted a factor of 2 (see equation (1)). The correct version of table 1 is presented here. This correction does not alter the subsequent discussions and conclusions, as all structures and facets lacked the factor of 2, and were compared relative to each other.

Table 1. Surface energy for the low index facets, (100), (110), (111), in the uniformly disordered structure, ordered structure, and ordered structure with a local inverse spinel cation ordering near the surface. Whenever a facet exhibits the same elements for different termination layers, we distinguish the slab cells by surface composition. In the uniformly disordered structure, the (110) surface composition Li:Mn:Ni is 1:2:1 and 1:1.5:0.5 in Li/Ni/Mn/O-I and -II, respectively. In the ordered structure, the (110) surface compositions are 1:2:0.25, 1:2.5:0.5, and 1:2:1 in Li/Ni/Mn/O-I, -II, and -III, respectively.

Ordering	Facet	Termination	γ (J m^{-2})
Uniform	(100)	Li/Mn/Ni/O	1.07
		Mn/Ni/O	1.73
		Mn/O	1.66
	(110)	Li/Mn/Ni/O-I	2.34
		Li/Mn/Ni/O-II	1.55
	(111)	Li/Ni/O	0.87
		Li/Mn/O	2.06
		Mn/O	1.41
Ordered	(100)	Li/Mn/Ni/O	1.11
		Mn/Ni/O	1.43
	(110)	Li/Mn/Ni/O-I	1.50
		Li/Mn/Ni/O-II	1.71
		Li/Mn/Ni/O-III	1.58
	(111)	Li/Mn/Ni/O	1.33
		Mn/Ni/O	2.04
Ordered'	(100)	Li/Mn/Ni/O	1.59
	(110)	Li/Mn/Ni/O	1.82
	(111)	Li/O	1.09
		Li/Mn/O	1.23

Nanotechnology **24** (2013) 424007 (6pp) doi:10.1088/0957-4484/24/42/424007

First-principles study of the nano-scaling effect on the electrochemical behavior in $LiNi_{0.5}Mn_{1.5}O_4$

Eunseok Lee and Kristin A Persson

Environmental Energy Technologies Division, Lawrence Berkeley National Laboratory, CA 94720, USA

E-mail: eunseoklee@lbl.gov

Received 29 January 2013, in final form 31 January 2013
Published 25 September 2013
Online at stacks.iop.org/Nano/24/424007

Abstract

Nano-scaling of electrode materials is often used in battery applications to enhance performance, particularly relating to rate capability. However, for the high-voltage spinel $LiNi_{0.5}Mn_{1.5}O_4$ conflicting results have been reported on the benefits of nano-scaling. In this study, we present first-principles calculations to investigate the effect of nano-scaling on $LiNi_{0.5}Mn_{1.5}O_4$, specifically focusing on the roles and coupling between surface stability, cation ordering and phase behavior. We calculate and compare the surface energy for the low index facets (100), (110), and (111), and find that the most stable facet is dependent on the cation ordering at the surface layer. In this context, we predict a spontaneous surface reconstruction in the cation-ordered structure which leads to a deviation from the perfect surface cation ordering and results in an enhanced accessibility to solid solution behavior as a function of Li content. Our results imply that nano-scaling will be more beneficial for the cation-ordered structure, as compared to the disordered structure where the solid solution region is already intrinsically accessible for a broad range of Li concentrations.

(Some figures may appear in colour only in the online journal)

1. Introduction

Rechargeable energy storage through Li-ion battery (LIB) systems presents a promising solution to power the next generation electric vehicles. The electrochemical performance of LIBs is mainly set by the two composite electrodes, and hence it is important to optimize the intrinsic properties of the active materials to meet the demands for future sustainable transportation. The $LiNi_{0.5}Mn_{1.5}O_4$ ('LMNO') 'high-voltage' spinel cathode material has attracted attention due to its low materials cost, non-toxicity, and competitive electrochemical performance [1, 2]. In particular, LMNO combines high stability through its Mn content and the spinel structure [3–5] but exhibits less of the Mn^{3+}-related issues compared to the parent compound Mn spinel, $LiMn_2O_4$, as the redox center occurs on the Ni site alone [6–11]. The high operating voltage around 4.7 V [3–5, 12] increases the theoretical energy density of $LiNi_{0.5}Mn_{1.5}O_4$ as compared to $LiMn_2O_4$ from 440 to 686 Wh kg^{-1} [13].

Recently, it has become increasingly popular to optimize the performance of Li electrode materials through nano-scaling [14–21]. Nanometric materials tend to exhibit (1) increased rate capability due to larger surface to volume ratios and shorter Li-ion diffusion paths as the particle size is reduced [14–18] and (2) increased access to the Li-vacancy solid solution domain due to the changes in the solubility limit at the nano-scale [19]. The spinel material exhibits three-dimensional Li diffusion paths, which should promote very high diffusivity. Yet, the experimental evidence of nano-scaling effect on the $LiNi_{0.5}Mn_{1.5}O_4$ remains controversial. For example, Shaju *et al* synthesized nano-$LiNi_{0.5}Mn_{1.5}O_4$ particle by a resorcinol-formaldehyde assisted solution method and reported that the disordered nano-$LiNi_{0.5}Mn_{1.5}O_4$ exhibits superior rate capability [16]. Talyosef *et al* also reported that the use of nano-materials was advantageous for better rate capability in their comparative study of nano- and micro-particles of $LiNi_{0.5}Mn_{1.5}O_4$ [17]. Conversely, the highest rate capability on record for the

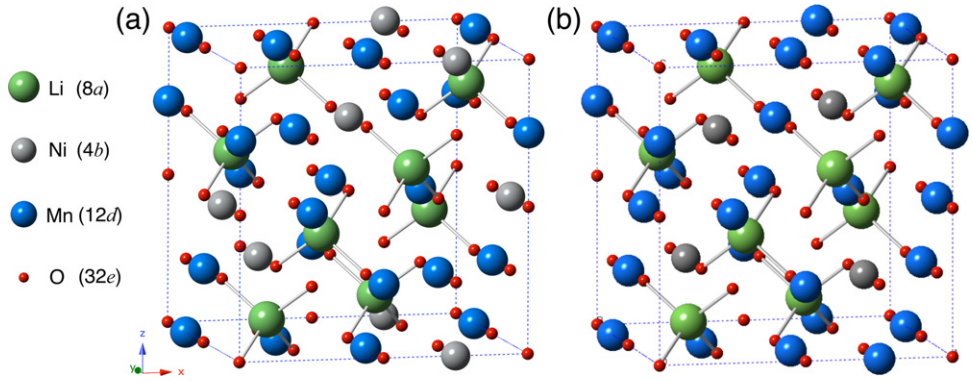

Figure 1. Unit cell of the $LiNi_{0.5}Mn_{1.5}O_4$ with the (a) ordered ($P4_332$) and (b) uniform cation arrangements. Wyckoff label: 8a-tetrahedral sites, 4b and 12d-octahedral sites.

high-voltage $LiNi_{0.5}Mn_{1.5}O_4$ spinel was reported by Ma *et al* using micronsized particles [18]. Another advantage of nano-scaling can be derived from design of phase behavior during cycling. A Li-vacancy solid solution reaction is generally preferred compared to extensive two-phase regions as it reduces the inherent strain in the material under cycling and promotes long life times. The change in the solubility limit and equilibrium compositions by nano-scaling can increase accessibility to the solid solution region and, hence, enhance the kinetic performance of electrode materials [19]. On the other hand, nanometric materials exhibit higher surface areas which increase the first-cycle capacity loss through the formation of solid–electrolyte interface and may continue to degrade the material through detrimental reactions with the electrolyte [20, 21].

In this paper, we perform the first-principles calculations based on the density functional theory to investigate nano-scaling effects in $LiNi_{0.5}Mn_{1.5}O_4$, with a focus on its surface stability, phase behavior and their dependence on the Ni–Mn cation ordering. We calculate and compare the surface energy for the low index facets and observe that the (111) facet is, intrinsically, the most stable in the disordered cation arrangement while the cation-ordered (111) surface region undergoes a significant cation reconstruction towards a local surface inverse spinel ordering without which, the (100) is the most stable surface facet. In our previous study [22], we have shown that any deviation of cation arrangement from the ideal Ni–Mn ordering improves the accessibility to the solid solution Li-vacancy phase. Our findings suggest that nano-scaling is likely to promote rate performance in the cation-ordered system, as the surface reconstruction results in a surface-layer transition to the solid solution, while the beneficial effect on the disordered high-voltage spinel where the Li-vacancy solid solution is already accessible in large parts of the phase diagram is perceived to be less pronounced.

2. Computational model and methodology

Depending on the synthesis process, the LMNO can have two overall cation arrangements, the ordered $P4_332$ and the disordered $Fd\bar{3}m$. As shown in figure 1(a), the ordered $LiNi_{0.5}Mn_{1.5}O_4$ exhibits Li 8a sites, Ni 4b sites, Mn 12d sites, and O 32e sites which result in an ionic configuration corresponding to the $P4_332$ space group. In the disordered $LiNi_{0.5}Mn_{1.5}O_4$, the Ni and Mn are distributed randomly at any of the 4b and 12d sites which result in an ionic configuration corresponding to the $Fd\bar{3}m$ space group. A randomly disordered Ni/Mn arrangement consists of a large number of different local Ni/Mn arrangements, compared to the (ideal) single Ni/Mn configuration in the ordered $P4_332$ structure. We note that representing a truly random Ni/Mn arrangement in the disordered structure requires an infinite (or very large) supercell. Instead, in this study we use a finite unit cell with uniformly distributed Ni and Mn ions forming a face-centered-cubic (fcc) sublattice as illustrated in figure 1(b). Previously, we showed [23, 22] that this 'uniformly disordered' configuration is the most representative local Ni/Mn arrangement within a random supercell in the disordered $Fd\bar{3}m$ $LiNi_{0.5}Mn_{1.5}O_4$ system due to its high occurrence as a local cation arrangement in any randomized Ni/Mn distribution as well as the its signature electrochemical profile.

For the ordered and uniformly disordered structures, we calculate the surface energy for the low index facets, (100), (110), and (111). The surface energy γ_i for a facet i is defined as

$$\gamma_i = \frac{E^i_{\text{slab}} - Ne_{\text{bulk}}}{2S_i} \tag{1}$$

where E^i_{slab} and e_{bulk} are the energy of a slab with surface facet i and the energy per atom of the bulk, respectively. N is the number of atoms in the slab and S_i is the surface area. The energy of the bulk material is calculated under periodic boundary conditions, assuming a ferrimagnetic state with $\uparrow$ and $\downarrow$ magnetic moments for Ni and Mn ions, respectively [23]. The supercell for the slab calculation is constructed by placing a slab at the center of the supercell with vacuum space normal to the surface of the slab. The vacuum thickness is set to 20 Å, which was found to be sufficient to remove interactions between the periodic slab images. The slab initial unit cell is obtained from the relaxed bulk structure as function of the termination composition. The bulk region within the slab is represented by fixing the atomic positions within the distance of 2.65 Å from the

center of slab in the direction of surface normal (total width of 5.3 Å, corresponding to 5–6 atomic layers). The atoms outside of this center region are allowed to fully relax. The (100), (110), and (111) facets fall within the type III surface category according to Tasker's criterion [24] which require a re-distribution of the ions at the surfaces and can result in significant reconstruction of the surface structure [24, 25]. For that purpose, we symmetrize the charged ions on the surface terminations to remove the dipoles while preserving overall stoichiometry. For each facet, the surface energy is calculated for all possible terminations and compared to identify the lowest surface energy termination. The equilibrium shape of the crystal is obtained by minimizing the total surface energy through the Wulff construction [26].

The total energy is obtained by first-principles electronic energy calculation based on the density functional theory. The spin-polarized generalized gradient approximation with Perdew–Burke–Ernzerhof parametrization for the exchange–correlation function [27, 28] and the projector augmented-wave (PAW) method [29, 30] are used as implemented in Vienna *ab initio* simulation package [31–34]. A high cutoff energy (520 eV) together with an adjusted *k*-point sampling, depending on the size of supercell, are used. We employ the $+U$ correction term to account for the electron localization around transition metal ions, e.g. 5.96 eV for Ni and 4.5 eV for Mn, respectively [35]. The oxidation state of each ion is determined by integrating the local magnetic moment within the Wigner–Seitz radius for each ion as given by the PAW method potentials.

Table 1. Surface energy for the low index facets, (100), (110), (111), in the uniformly disordered structure, ordered structure, and ordered structure with a local inverse spinel cation ordering near the surface. Whenever a facet exhibits the same elements for different termination layers, we distinguish the slab cells by surface composition. In the uniformly disordered structure, the (110) surface composition Li:Mn:Ni is 1:2:1 and 1:1.5:0.5 in Li/Ni/Mn/O-I and -II, respectively. In the ordered structure, the (110) surface compositions are 1:2:0.25, 1:2.5:0.5, and 1:2:1 in Li/Ni/Mn/O-I, -II, and -III, respectively.

Ordering	Facet	Termination	γ (J m^{-2})
Uniform	(100)	Li/Mn/Ni/O	2.13
		Mn/Ni/O	3.45
		Mn/O	3.31
	(110)	Li/Mn/Ni/O-I	4.67
		Li/Mn/Ni/O-II	3.10
	(111)	Li/Ni/O	1.74
		Li/Mn/O	4.12
		Mn/O	2.83
Ordered	(100)	Li/Mn/Ni/O	2.22
		Mn/Ni/O	2.86
	(110)	Li/Mn/Ni/O-I	3.00
		Li/Mn/Ni/O-II	3.41
		Li/Mn/Ni/O-III	3.16
	(111)	Li/Mn/Ni/O	2.67
		Mn/Ni/O	4.08
Ordered′	(100)	Li/Mn/Ni/O	3.19
	(110)	Li/Mn/Ni/O	3.63
	(111)	Li/O	2.18
		Li/Mn/O	2.45

3. Result and discussion

The calculated surface energies for the (100), (110), and (111) facets in the uniformly disordered and ordered structures are presented in table 1. For the (110) facets, in both the ordered as well as the uniformly disordered structures, the termination layer contains all the elements Li, Mn, Ni, and O and hence they are classified by the termination layer composition, see table 1. We observe that, for the same facet and comparing the surface energies for different surface compositions (see table 1) the surface energy decreases (stabilizes) with more Li ions and less Mn/Ni ions in the termination layer. This is intuitive as Li has lower coordination than Ni and Mn and thus the number of broken bonds per area will be fewer than that for Ni and Mn. For the uniformly disordered structure (the most highly occurring local ordering in the disordered spinel with random cation arrangements), the (111) facet with Li/Ni/O-termination has the lowest surface energy among the investigated facets, which agrees with several existing experimental observations [1, 3]. For the ordered structure, however, using only the atomic rearrangement required to remove the dipole moment and routine cell relaxations, the (100) facet with the Li/Mn/Ni/O-termination is predicted to be most stable, which contrasts with experimental observations [1, 3]. We speculate that the discrepancy between our computational prediction and existing experimental observations is due to a significant surface reconstruction, as suggested in previous computational studies on the $LiMn_2O_4$ by Karim *et al* [25] and Benedek *et al* [36]. In these works, the calculated (111) surface energy of $LiMn_2O_4$ was found to be higher (more unstable) than that of (100), although experimental observations agree that the (111) facet dominate most spinel equilibrium particle morphologies. However, Karim *et al* also observed that the surface energy of the (111) facet can be drastically lowered compared to that of (100) facet if a targeted surface cation reconstruction is employed where the Mn ions on the surface are locally swapped with the Li ions in the next available layer leading to a local inverse spinel cation arrangement near the surface. This finding is consistent with previous works for different materials [37, 38] where lower charged cations on the surface with a smaller loss in coordination generally result in a reduction of the surface energy. We applied this targeted reconstruction technique to the (111) facet of the ordered $LiNi_{0.5}Mn_{1.5}O_4$ by swapping the Ni and Mn ions on the surface with the Li ions in the next available layer. The result is presented in table 1 (see the data for 'Ordered′') where we note that the (111) facet with local inverse spinel cation ordering, e.g. Li/O-termination, has the lowest surface energy (lower than that of the (100) facet with Li/Mn/Ni/O-termination in the unaltered ordered structure). We also examined the (111) Li/Mn/O-termination where only the Ni ions are swapped with the Li ions in the next available layer. The surface energy of this termination was found to be higher than the complete Mn/Ni surface inverse spinel reconstruction but lower than the original Li/Mn/Ni/O ordered structure, which indicates a continuous trend where the surface energy decreases as a function of

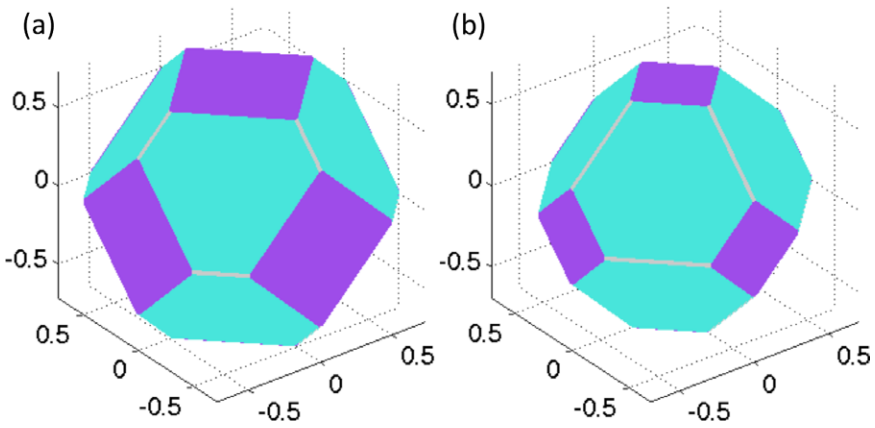

Figure 2. The equilibrium particle shape of (a) the ordered structure with a local inverse spinel surface structure with $\gamma_{\text{total}} = 1.36$ J and (b) the uniformly disordered structure with $\gamma_{\text{total}} = 1.04$ J. The (100), (110), and (111) facets are depicted using the colors violet, gray, and turquoise, respectively.

exchanging surface Ni/Mn for bulk Li for the (111) surface. Thus, our findings suggest that the ordered structure will undergo a significant spontaneous surface reconstruction (see table 1). We also found that only the (111) facet reduces its surface energy by this local cation inversion. For the (100) and (110) facets, the surface energy actually increases with the swapping, which means that the surface reconstruction decreases the stability of the original (100) and (110) surfaces. We believe this is the result of a trade-off between the surface bonding energy loss and the energy loss due to the less favorable (inverse spinel) cation arrangement as we have previously shown that the ordered Ni/Mn spinel structure corresponds to the lowest energy cation arrangement [23, 22]. Even for the (111) facet, the reduction of the surface energy by the cation inversion reconstruction is not as drastic as that for the Mn spinel, $LiMn_2O_4$, which exhibits a change in the surface energy from 1.39 to 0.65 J m^{-2}. Comparing the two related cases, we ascribe this difference to the strong cation ordering in the fully lithiated $LiNi_{0.5}Mn_{1.5}O_4$ [23, 22] structure as compared to the Mn spinel which exhibits significant internal structural frustration due to competing charge, Jahn–Teller and magnetic orderings [39, 40]. The equilibrium crystal shape is obtained by minimizing the total surface energy through the Wulff construction. The surface energy data in table 1 is used and the resulting equilibrium crystal shapes for both the reconstructed ordered as well as the uniformly disordered structures are illustrated in figure 2. As the (111) surface exhibits the lowest energy in both cases, the (111) facet dominates the particle morphology, followed by the (100) and (110) facets resulting in cubo-octahedral shapes in agreement with experimental observations [1, 3, 20]. The surface reconstruction in the ordered compound leads us to an interesting hypothesis of the nano-scaling effects on the properties of LMNO, particularly related to its phase behavior during Li insertion/deinsertion. As the ordered surface region reconstructs, the cation arrangement of surface region deviates from the ideal ordered structure. According to our previous study, the Li insertion/extraction in the ordered structure is governed by an extensive two-phase reaction between coexistent $\square Ni_{0.5}Mn_{1.5}O_4$ and $LiNi_{0.5}Mn_{1.5}O_4$ phases. However, any deviation from the ideal ordered structure enhances accessibility to the solid solution region [22]. It is generally accepted that solid solution behavior during cycling is preferred in order to promote rate capability as the energy barrier due to the nucleation and growth in the two-phase region is bypassed and thus we expect that kinetic performance near the reconstructed surface region to be improved. Consequently, using nano-scaling to increase the surface to bulk ratio should correlate with a kinetically improved region for the ordered structure as compared to larger particles. On the other hand, the uniformly disordered structure exhibits no significant (111) surface reconstruction and already shows predominantly solid solution behavior, especially at high Li content [22]. Hence, we expect a stronger correlation between nano-scaling, improved accessibility to the solid solution region and improved rate performance for the ordered LMNO material as compared to the disordered ($Fd\bar{3}m$) material.

4. Conclusion

In summary, we calculated the surface energy as a function of facet and surface termination in the cation-ordered and disordered high-voltage Ni–Mn spinel ($LiNi_{0.5}Mn_{1.5}O_4$). Employing a local uniform cation distribution as a proxy for the disordered ($Fd\bar{3}m$) material, we found the (111) surface to be the dominant facet. However, for the ordered material, the (111) surface only stabilizes with respect to the other low index (100) and (110) surface facets by undergoing a target local cation inversion reconstruction where surface Mn/Ni ions are exchanged with bulk Li ions in the next available layer. Thus, our calculations predict that the (111) facet is the most stable surface facet (followed by the (100) and the (110) facets) for both the ordered as well as the disordered LMNO materials, resulting in an equilibrium cubo-octahedral particle morphology, in agreement with experimental observations. The surface reconstruction in the ordered material results in a deviation from the ideal ordered cation arrangement, which will (according to previous studies) result in an enhanced accessibility to the Li-vacancy solid solution region. However,

the uniformly disordered structure exhibits no significant (111) surface reconstruction and already shows predominant solid solution behavior, especially at high Li content. Thus, based on our findings, we propose that increasing the surface to bulk ratio through nano-scaling is likely to correlate favorably with improved properties, e.g. rate capability, for the ordered structure but less so for the disordered material.

Acknowledgments

Work at the Lawrence Berkeley National Laboratory was supported by the Assistant Secretary for Energy Efficiency and Renewable Energy, Office of Vehicle Technologies of the US Department of Energy, under Contract No. DE-AC02-05CH11231. We are also grateful to Cheonjoong Kim and Jordi Cabana for enlightening discussions on the high-voltage spinel.

References

[1] Kim J-H, Myung S-T, Yoon C S, Kang S G and Sun Y-K 2004 Comparative study of $LiNi_{0.5}Mn_{1.5}O_{4-\delta}$ and $LiNi_{0.5}Mn_{1.5}O_4$ cathodes having two crystallographic structures: $Fd\bar{3}m$ and $P4_332$ *Chem. Mater.* **16** 906

[2] Shu J, Yi T-F, Shui M, Wang Y, Zhu R-S, Chu X-F, Huang F, Xu D and Hou L 2010 Comparison of electronic property and structural stability of $LiMn_2O_4$ and $LiNi_{0.5}Mn_{1.5}O_4$ as cathode materials for lithium-ion batteries *Comput. Mater. Sci.* **50** 776–9

[3] Xia H, Meng Y S, Lu L and Ceder G 2007 Electrochemical properties of nonstoichiometric $LiNi_{0.5}Mn_{1.5}O_{4-\delta}$ thin-film electrodes prepared by pulsed laser deposition *J. Electrochem. Soc.* **154** A737

[4] Mohamedi M, Makino M, Dokko K, Itoh T and Uchida I 2002 Electrochemical investigation of $LiNi_{0.5}Mn_{1.5}O_4$ thin film intercalation electrodes *Electrochim. Acta* **48** 79–84

[5] Xiao J *et al* 2012 High-performance $LiNi_{0.5}Mn_{1.5}O_4$ spinel controlled by Mn^{3+} concentration and site disorder *Adv. Mater.* **24** 2109–16

[6] Xia H, Tang S B, Lu L, Meng Y S and Ceder G 2007 The influence of preparation conditions on electrochemical properties of $LiNi_{0.5}Mn_{1.5}O_4$ thin film electrodes by PLD *Electrochim. Acta* **52** 2822–8

[7] Xia Y, Sakai T, Fujieda T, Yang X Q, Sun X, Ma Z F, McBreen J and Yoshio M 2001 Correlating capacity fading and structural changes in $Li_{1+y}Mn_{2-y}O_{4-\delta}$ spinel cathode materials: a systematic study on the effects of Li/Mn ratio and oxygen deficiency *J. Electrochem. Soc.* **148** A723–9

[8] Benedek R and Thackeray M M 2006 Reaction energy for $LiMn_2O_4$ spinel dissolution in acid *Electrochem. Solid-State Lett.* **9** A265–7

[9] Wei Y J, Yan L Y, Wang C Z, Xu X G, Wu F and Chen G 2004 Effects of Ni doping on $[MnO_6]$ octahedron in $LiMn_2O_4$ *J. Phys. Chem.* B **108** 18547–51

[10] Singh G, Gupta S L, Prasad R, Auluck S, Gupta R and Sil A 2009 Suppression of Jahn–Teller distortion by chromium and magnesium doping in spinel $LiMn_2O_4$: a first-principles study using GGA and GGA + *U* *J. Phys. Chem. Solids* **70** 1200–6

[11] Verhoeven V W J, Mulder F M and de Schepper I M 2000 Influence of Mn by Li substitution on the Jahn–Teller distortion in $LiMn_2O_4$ *Physica* B **276–278** 950–1

[12] Park S-H and Sun Y-K 2004 Synthesis and electrochemical properties of 5 V spinel $LiNi_{0.5}Mn_{1.5}O_4$ cathode materials prepared by ultrasonic spray pyrolysis method *Electrochim. Acta* **50** 434–9

[13] Liu G Q, Wen L and Liu Y M 2010 Spinel $LiNi_{0.5}Mn_{1.5}O_4$ and its derivatives as cathodes for high-voltage Li-ion batteries *J. Solid State Electrochem.* **14** 2191–202

[14] Malik R, Burch D, Bazant M and Ceder G 2010 Particle size dependence of the ionic diffusivity *Nano Lett.* **10** 4123–7

[15] Arrebola J C, Caballero A, Cruz M, Hernán L, Morales J and Castellón E R 2006 Crystallinity control of a nanostructured $LiNi_{0.5}Mn_{1.5}O_4$ spinel via polymer-assisted synthesis: a method for improving its rate capability and performance in 5 V lithium batteries *Adv. Funct. Mater.* **16** 1904–12

[16] Shaju K M and Bruce P G 2008 Nano-$LiNi_{0.5}Mn_{1.5}O_4$ spinel: a high power electrode for Li-ion batteries *Dalton Trans.* **0** 5471–5

[17] Talyosef Y, Markovsky B, Lavi R, Salitra G, Aurbach D, Kovacheva D, Gorova M, Zhecheva E and Stoyanova R 2007 Comparing the behavior of nano- and microsized particles of $LiNi_{0.5}Mn_{1.5}O_4$ spinel as cathode materials for Li-ion batteries *J. Electrochem. Soc.* **154** A682–91

[18] Ma X, Kang B and Ceder G 2010 High rate micron-sized ordered $LiNi_{0.5}Mn_{1.5}O_4$ *J. Electrochem. Soc.* **157** A925–31

[19] Wagemaker M, Mulder F M and Van der Ven A 2009 The role of surface and interface energy on phase stability of nanosized insertion compounds *Adv. Mater.* **21** 2703–9

[20] Chen Z, Qiu S, Cao Y, Ai X, Xie K, Hong X and Yang H 2012 Surface-oriented and nanoflake-stacked $LiNi_{0.5}Mn_{1.5}O_4$ spinel for high-rate and long-cycle-life lithium ion batteries *J. Mater. Chem.* **22** 17768–72

[21] Lafont U, Locati C and Kelder E M 2006 Nanopowders of spinel-type electrode materials for Li-ion batteries *Proc. E-MRS Symp. P on Solid State Ionics: Mass and Charge Transport at Various Length Scales; Solid State Ion.* **177** 3023–9

[22] Lee E and Persson K A 2013 Design of room temperature solid-solution Li extraction/insertion materials through target cation disorder, submitted

[23] Lee E and Persson K A 2012 Revealing the coupled cation interactions behind the electrochemical profile of $Li_xNi_{0.5}Mn_{1.5}O_4$ *Energy Environ. Sci.* **5** 6047–51

[24] Tasker P W 1979 The stability of ionic crystal surface *J. Phys. C: Solid State Phys.* **12** 4977

[25] Karim A, Fosse S and Persson K A 2013 The surface structure and equilibrium particle shape of the $LiMn_2O_4$ spinel from first-principles calculations *Phys. Rev.* B at press

[26] Wulff G 1901 On the question of the rate of growth and dissolution of crystal surfaces *Z. Kristallogr. Mineral.* **34** 449–530

[27] Perdew J P, Burke K and Ernzerhof M 1997 Erratum: generalized gradient approximation made simple *Phys. Rev. Lett.* **78** 1396

[28] Perdew J P, Burke K and Ernzerhof M 1996 Generalized gradient approximation made simple *Phys. Rev. Lett.* **77** 3865

[29] Kresse G and Joubert D 1999 From ultrasoft pseudopotentials to the projector augmented-wave method *Phys. Rev.* B **59** 1758

[30] Blöchl P E 1994 Projector augmented-wave method *Phys. Rev.* B **50** 17953

[31] Kresse G and Furthmüller J 1996 Efficiency of *ab initio* total energy calculations for metals and semiconductors using a plane-wave basis set *Comput. Mater. Sci.* **6** 15–50

[32] Kresse G and Furthmüller J 1996 Efficient iterative schemes for *ab initio* total-energy calculations using a plane-wave basis set *Phys. Rev.* B **54** 11169

[33] Kresse G and Hafner J 1994 *Ab initio* molecular-dynamics simulation of the liquid–metal–amorphous–semiconductor transition in germanium *Phys. Rev.* B **49** 14251

[34] Kresse G and Hafner J 1993 *Ab initio* molecular dynamics for liquid metals *Phys. Rev.* B **47** 558

[35] Zhou F, Cococcioni M, Marianetti C A, Morgan D and Ceder G 2004 First-principles prediction of redox potentials in transition-metal compounds with LDA + *U* *Phys. Rev.* B **70** 235121

[36] Benedek R and Thackeray M M 2011 Simulation of the surface structure of lithium manganese oxide spinel *Phys. Rev.* B **83** 195439

[37] Persson K A, Waldwick B, Lazic P and Ceder G 2012 Prediction of solid–aqueous equilibria: scheme to combine first-principles calculations of solids with experimental aqueous states *Phys. Rev.* B **85** 235438

[38] Kramer D and Ceder G 2009 Tailoring the morphology of $LiCoO_2$: a first principles study *Chem. Mater.* **21** 3799–809

[39] Ouyang C Y, Shi S Q and Lei M S 2009 Jahn–Teller distortion and electronic structure of $LiMn_2O_4$ *J. Alloys Compounds* **474** 370–4

[40] Tomeno I, Kasuya Y and Tsunoda Y 2001 Charge and spin ordering in $LiMn_2O_4$ *Phys. Rev.* B **64** 094422